Journal of Alloys and Compounds 509 (2011) 3070–3073

Contents lists available at ScienceDirect

Journal of Alloys and Compounds

journal homepage: www.elsevier.com/locate/jallcom

Broadband near-infrared emission in Er^{3+}–Tm^{3+} co-doped bismuthate glasses

Kefeng Li[a,b,*], Huiyan Fan[a,b], Guang Zhang[a,b], Gongxun Bai[a,b], Sijun Fan[a,b], Junjie Zhang[a], Lili Hu[a]

[a] Key Laboratory of Materials for High Power Laser, Shanghai Institute of Optics and Fine Mechanics, Chinese Academy of Sciences, Shanghai 201800, PR China
[b] Graduate School of Chinese Academy of Sciences, Beijing 100039, PR China

ARTICLE INFO

Article history:
Received 10 September 2010
Received in revised form
29 November 2010
Accepted 30 November 2010
Available online 8 December 2010

Keywords:
Bismuthate glass
Er^{3+}–Tm^{3+} codoping
Broadband emission
Temperature dependence

ABSTRACT

In this work, we report near infrared emission spectra of Er^{3+}–Tm^{3+} co-doped Bi_2O_3–GeO_2–Na_2O (BGN) glasses with the excitation of 800 nm laser. A broad emission extending from 1300 to 1650 nm with a full width at half maximum (FWHM) of ~160 nm is obtained in a 1.0 wt% Tm_2O_3 and 0.3 wt% Er_2O_3 co-doped BGN glass. The energy transfer processes between Tm^{3+} and Er^{3+} in BGN glasses are analyzed in detail. The temperature dependence of the broadband emission spectra in Er^{3+}–Tm^{3+} co-doped BGN glass is also studied. The present work indicates that Er^{3+}–Tm^{3+} co-doped BGN glasses can be promising materials for broadband light sources and broadband amplifiers for WDM transmission systems.

1. Introduction

In the past decade, the broadband optical amplification beyond the conventional 1.5 μm window of Er-doped fiber amplifier (EDFA) is of interest for the increasing demands of information traffic, which requires the development of wide band integrated amplifiers in order to increase the transmission capacity of wavelength division multiplexing (WDM) systems [1]. Moreover, broadband light sources are a prerequisite for the application of optical coherence tomography [2]. A logical route would be addition of other rare earth (RE) such as Tm^{3+} to achieve such broadband emission with overlapping emission bands [3]. The $^3H_4 \rightarrow {}^3H_6$ transition of Tm^{3+} ions at around 1460 nm provides an excellent complement to Er^{3+} ions. Jeong et al. had demonstrated an Er^{3+}–Tm^{3+} co-doped 20 m long silica fiber amplifier spontaneous emission (ASE) with bandwidth over 90 nm (1460–1550 nm), when the fiber is pumped at 980 nm [4], however, it should be taken into account that the emission originates at the $^3H_4$ level has a relatively small gap to the $^3H_5$ level (~4300 cm^{-1}), and as a consequence nonradiative recombination to this level is favored in silica and most silica based glasses because of the high maximum phonon energy (MPE) (~1100 cm^{-1}) [5]. Therefore, researches have been focused on the low-phonon energy materials, such as fluoride (MPE ~550 cm^{-1}) [6], chalcogenide (MPE ~350 cm^{-1}) [7], tellurite glasses (MPE ~750 cm^{-1}) [8,9] and oxyfluoride glass ceramics [10]. Nevertheless, to the best of our knowledge, there has not been any report on the broadband emission in Er^{3+}–Tm^{3+} co-doped bismuthate glasses.

Bismuthate glasses have important advantages for optical (including structure) and electrical properties over other common oxide glasses [11–15]. Our previous work indicated that bismuthate glass (Bi_2O_3–GeO_2–Na_2O) has a phonon energy of ~440 cm^{-1}, which is significantly lower than both silicates and tellurites [12], and comparable to chalcogenides [16]. This extends the infrared transparency range to ~6 μm [12,13] and results in lower non-radiative rates, which is helpful to reduce the multiphonon relaxation from $^3H_4$ level to $^3H_5$ level. Bismuthate glass also exhibits high rare earth ions solubility, enabling highly doped and hence very compact fiber lasers to be produced [17]. The large refractive index (~2.1) of bismuthate glass enhances both the absorption and emission cross sections [12]. On the other hand, it is well known that Bi_2O_3 is a conditional glass network former [11,18–20], the presence of two glass formers Bi_2O_3 and GeO_2 produce a more complex network structure with a great variety of sites for the RE ions which contribute to the inhomogeneous broadening of the emission band. Moreover, bismuthate glasses are more chemically and environmentally stable than fluoride glasses and have the advantages of oxide glass fabrication techniques. Finally, the PbO-free glass composition is nontoxic to environment. In the present work, a broad and flat emission extending from 1300 nm to 1650 nm in Er^{3+}–Tm^{3+} co-doped bismuthate glass was observed using the pump excitation at 800 nm. The visible upconversion emission spectra were recorded to understand the

* Corresponding author at: Key Laboratory of Materials for High Power Laser, Shanghai Institute of Optics and Fine Mechanics, Chinese Academy of Sciences, P.O. Box 800-211, Shanghai 201800, PR China. Tel.: +86 21 59914293; fax: +86 21 59914516.
E-mail address: kfli@siom.ac.cn (K. Li).

0925-8388/$ – see front matter © 2010 Elsevier B.V. All rights reserved.
doi:10.1016/j.jallcom.2010.11.201

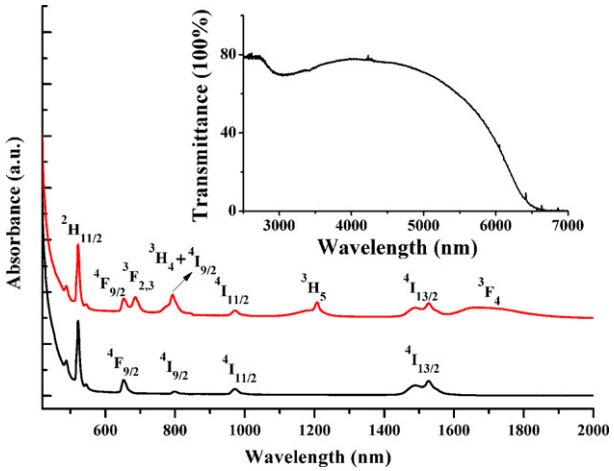

Fig. 1. Room temperature absorption spectra of BGNEr and BGNEr3Tm glasses. The inset is the IR transmittance spectrum of un-doped BGN glass.

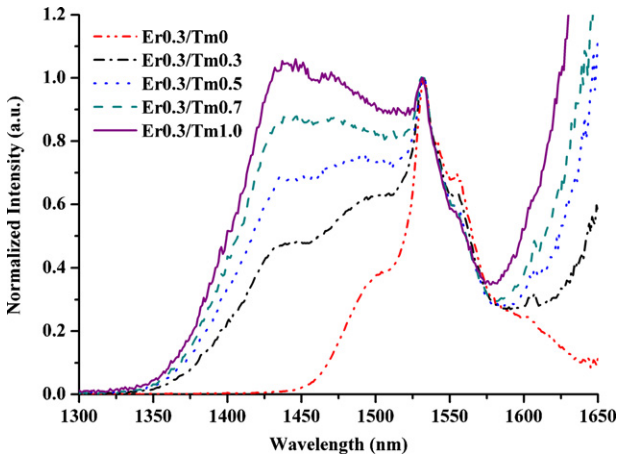

Fig. 2. Room temperature emission spectra of Er^{3+} singly doped and co-doped with Tm^{3+} BGN glasses with the excitation of 800 nm laser.

luminescence mechanism. The temperature dependence of luminescence in Er^{3+}–Tm^{3+} co-doped bismuthate glass is investigated. The energy transfer processes between Er^{3+} and Tm^{3+} are discussed.

2. Experimental

The glasses with the composition of $50Bi_2O_3$–$40GeO_2$–$10Na_2O$ (BGN) were prepared by conventional melt-quenching method. The doping concentration of Er^{3+} in the doped glass was 0.3 wt%, while the Er^{3+}–Tm^{3+} codoped bismuthate glasses had a fixed concentration of 0.3 wt% Er_2O_3 and different concentrations of Tm_2O_3: 0.3, 0.5, 0.7, and 1.0 wt%, respectively. The starting materials Bi_2O_3, GeO_2, Tm_2O_3 and Er_2O_3 are high purity reagents (99.99% minimum), and Na_2CO_3 with 99.9% purity. The glasses obtained hereafter are denoted as BGNEr, BGNEr3Tm, BGNEr5Tm, BGNEr7Tm, and BGNEr10Tm. Approximately 20 g powder is thoroughly mixed and melted in a platinum crucible at 1100 °C for 30 min with a closed lid and bubbled with dry O_2. The melt is casted at 1050 °C into a stainless steel mold and annealed at 400 °C for 3 h. All the samples were cut and polished to $10 \times 10 \times 1\,mm^3$ for spectroscopic measurements.

The absorption spectra were recorded with a Perkin-Elmer Lambda 900 UV/VIS/NIR spectrophotometer in the range of 400–2000 nm. Infrared (IR) transmittance was measured by a thermo nicolet (Nexus FT-IR spectrometer) spectrophotometer. The near infrared luminescence signals were detected with InP/InGaAs photomultiplier (PMT, R5509) excited by a 800 nm LD. Upconversion emission was detected with InP/InGaAs photomultiplier (PMT, R928) excited by a 800 nm LD. The fluorescence decay curves were recorded with a NIR MPT (R5509) excited by a microsecond flash lamp (μF 900). For the sample BGNEr10Tm, the broadband near infrared emission spectra and the fluorescence decay curves in the 10–300 K were collected.

3. Results and discussion

3.1. The absorption/IR transmittance spectra and Judd–Ofelt analysis

The room temperature absorption spectra were obtained for all samples in the range of 400–2000 nm, as an example, Fig. 1 shows the absorption spectra of BGNEr and BGNEr3Tm glasses, the inset is the IR transmittance spectrum of un-doped BGN glass. The IR transmittance reaches ~5.5 μm. The spectrum of the co-doped sample is characterized by the transition bands from the Er^{3+} $^4I_{15/2}$ ground state to the different higher levels $^4F_{7/2}$, $^2H_{11/2}$, $^3S_{3/2}$, $^4F_{9/2}$, $^4I_{9/2}$, $^4I_{11/2}$, and $^4I_{13/2}$, together with the Tm^{3+} absorption bands from the $^3H_6$ ground state to higher levels. The band positions for Er^{3+} and Tm^{3+} are similar to tellurite glasses [9]. The absorption spectra are similar for all the samples used in this study and the absorbance for different absorption bands shows linear dependence on the concentrations of Tm^{3+} and Er^{3+} ions in the samples.

According to the Judd–Ofelt theory [21,22], the J–O intensity parameters for both Er^{3+} and Tm^{3+} are listed in Table 1 and compared to some of the values available in literatures. The order of the Judd–Ofelt parameters is $\Omega_2 > \Omega_4 > \Omega_6$ for both Er: BGN and Tm: BGN. It is well know that Ω_2 is the most sensitive to the covalent bonding [23], so we can reasonable deduce that the covalent degree of the present BGN is stronger than fluoride and tellurite glasses. On the other hand, the Ω_4/Ω_6 determines the spectroscopy quality of the host materials [27], it is clear that the present BGN glass has a value of Ω_4/Ω_6 comparable with other glasses listed in Table 1, which suggests that BGN glass is a good matrix for infrared emission.

3.2. Emission spectra at room temperature

Fig. 2 shows the normalized near infrared emission spectra of Er^{3+} single doped and Er^{3+}–Tm^{3+} co-doped BGN glasses by exciting at 800 nm. For the Er^{3+} single doped glass, the emission is attributed to $^4I_{13/2} \rightarrow {}^4I_{15/2}$ transition with a full width at half-maximum (FWHM) of ~50 nm. The emission spectra of the co-doped samples shows the $^3H_4 \rightarrow {}^3F_4$ and $^4I_{13/2} \rightarrow {}^4I_{15/2}$ transitions of Tm^{3+} and Er^{3+} ions, respectively, together with the short wavelength tail of the Tm emission due to $^3F_4 \rightarrow {}^3H_6$ transition. We cannot observe this transition because of the upper limit of the detector at 1650 nm. With the increasing addition of Tm_2O_3, the emission spectra broaden sig-

Table 1
The Judd–Ofelt parameters of Er^{3+} and Tm^{3+} in BGN and various other glass matrices.

Glasses	RE ion concentration (10^{20} ions/cm^3)	Ω_2 (10^{-20} cm^2)	Ω_4 (10^{-20} cm^2)	Ω_6 (10^{-20} cm^2)	Ω_4/Ω_6	Reference
Er: BGN	0.415	6.51	2.11	1.52	1.39	This work
Germanate	2.3	7.2	1.3	1.1	1.18	[24]
Fluoride	–	2.98	1.40	1.04	1.35	[25]
Tellurite	–	5.93	1.50	1.07	1.40	[26]
Tm: BGN	1.383	5.11	2.38	1.68	1.42	This work
Germanate	–	5.55	2.03	1.26	1.61	[27]
Fluoride	–	1.96	1.36	1.16	1.17	[27]
Tellurite	3.76	4.48	1.87	1.30	1.44	[27]

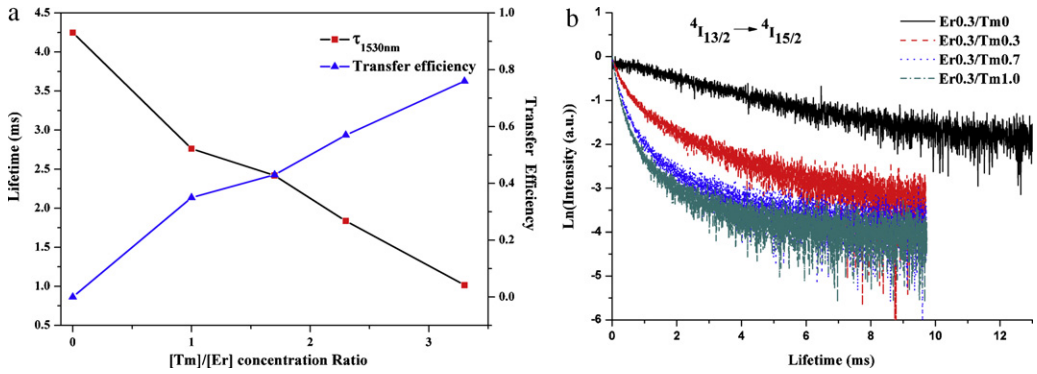

Fig. 3. (a) Lifetimes of the $^4I_{13/2} \rightarrow {}^4I_{15/2}$ emission (■) and Er^{3+}–Tm^{3+} energy transfer efficiency (▲) as a function of Tm^{3+} concentration including zero. (b) Logarithmic plot of the fluorescence decays of the $^4I_{13/2} \rightarrow {}^4I_{15/2}$ emission as a function of Tm^{3+} concentration.

nificantly, it is clear to see from Fig. 2 that the emission at 1460 nm, which is corresponding to $^3H_4 \rightarrow {}^3F_4$ transition, becomes stronger with the increasing concentration of Tm^{3+} ions. The intensity balance between the $^3H_4 \rightarrow {}^3F_4$ and $^4I_{13/2} \rightarrow {}^4I_{15/2}$ transitions become nearly equal to unity for a sample doped with 0.3 wt% of Er_2O_3 and 1.0 wt% of Tm_2O_3. The emission of this sample has a full width at half maximum (FWHM) ~160 nm, which is much larger than that of Er^{3+}–Tm^{3+} co-doped silica fiber (90 nm) [4], and comparable to that reported ~160 nm in Er^{3+}–Tm^{3+} co-doped TeO_2–WO_3–PbO glass [3] and 175 nm in oxyfluoride silicate glass ceramic [10]. The FWHM of 160 nm is also comparable to the largest value of ~160 nm in Er^{3+}–Tm^{3+} co-doped tellurite fiber [8]. Furthermore, the lower phonon energy environment of rare earth ions in the present bismuthate glasses makes it more suitable for the application in the WDM transmission systems [10].

The decay curves of Tm^{3+}:1460 nm and Er^{3+}:1530 nm of the samples were obtained under microsecond flash lamp (μF 900) excitation at 800 nm. Fig. 3(a) shows the lifetime values of $^4I_{13/2}$ level in the single doped and co-doped samples with fixed 0.3 wt% of Er_2O_3. It can be seen that the lifetime of $^4I_{13/2}$ level reduces greatly by codoping with Tm^{3+}, which means the efficient energy transfer from Er^{3+} to Tm^{3+}. The energy transfer efficiency η from Er^{3+} to Tm^{3+} can be expressed as [3]

$$\eta = 1 - \frac{\tau_{Er-Tm}}{\tau_{Er}}, \quad (1)$$

where τ_{Er-Tm} and τ_{Er} are the lifetimes of $^4I_{13/2}$ level with and without Tm^{3+} codoping. Fig. 3(a) also shows the Er → Tm energy transfer efficiencies for the co-doped samples. In BGNEr10Tm glass, the energy transfer efficiency from Er^{3+} to Tm^{3+} is 77%, which is comparable to that reported in TeO_2–WO_3–PbO glass [3] and tellurite fiber [8]. Fig. 3(b) shows the Ln (Intensity (a.u.)) versus lifetime in Er^{3+} single doped and Er^{3+}–Tm^{3+} co-doped samples, it is found that that the decay curves of Er^{3+} in BGNEr is approximately single-exponential, however, for the sample codoping with Tm^{3+}, the decay curve becomes nonsingle-exponential obviously, which indicates the efficient energy transfer from Er^{3+} to Tm^{3+}.

Fig. 4 shows the upconversion spectra of Er^{3+} doped and Er^{3+}/Tm^{3+} co-doped BGN glasses, which were also measured at room temperature under 800 nm LD excitation. For the Er^{3+} single doped BGN glass, the excitation from $^4I_{15/2}$ to $^4I_{9/2}$ generates green fluorescence $^2H_{11/2} \rightarrow {}^4I_{15/2}$ (525 nm), $^4S_{3/2} \rightarrow {}^4I_{15/2}$ (545 nm), and $^4F_{9/2} \rightarrow {}^4I_{15/2}$ (665 nm) due to the excited state absorption (ESA) and the energy transfer upconversion (ETU) processes similar to those reported in tellurite glass and oxyfluoride silicate glass ceramic [3,10]. For the Er^{3+}/Tm^{3+} co-doped glasses, the intensities of green emissions reduce significantly as Tm^{3+} concentration increases, while the intensity of red emission increases slightly. The intensities of green and red emissions affected via the addition of

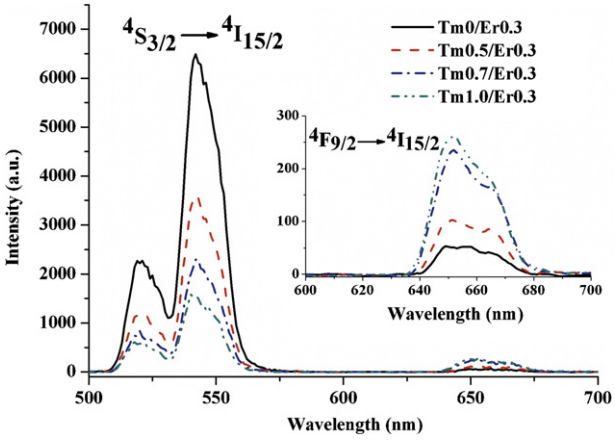

Fig. 4. Upconversion emission spectra of Er^{3+} ions in the single doped and co-doped BGN glasses.

Tm^{3+} into Er^{3+} doped BGN glasses, which indicates the presence of efficient energy transfer between both ions [3].

3.3. Temperature dependence of the broadband emission spectra

Fig. 5 shows the temperature dependence of the emission spectra corresponding to $^3H_4 \rightarrow {}^3F_4$ and $^4I_{13/2} \rightarrow {}^4I_{15/2}$ transitions between 10 K and 300 K for the sample BGNEr10Tm. The inset is the measured lifetimes of $^4I_{13/2}$ and $^3H_4$ changed with tempera-

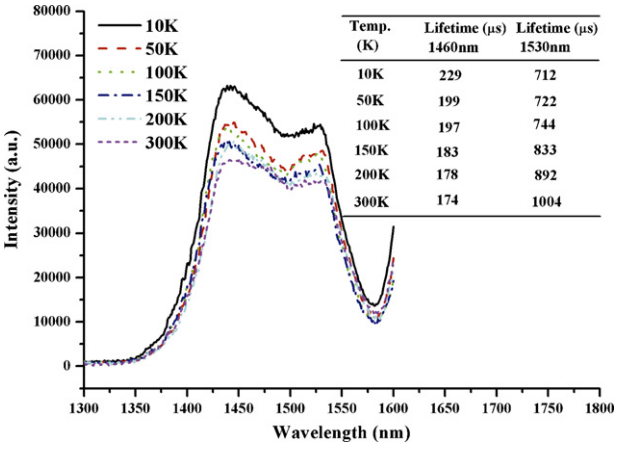

Temp. (K)	Lifetime (μs) 1460nm	Lifetime (μs) 1530nm
10K	229	712
50K	199	722
100K	197	744
150K	183	833
200K	178	892
300K	174	1004

Fig. 5. Temperature dependence of the broadband emission spectra of BGNEr10Tm glass in the range of 10–300 K. The inset shows the temperature dependence of the lifetimes of Er^{3+} (1.53 μm) and Tm^{3+} (1.46 μm).

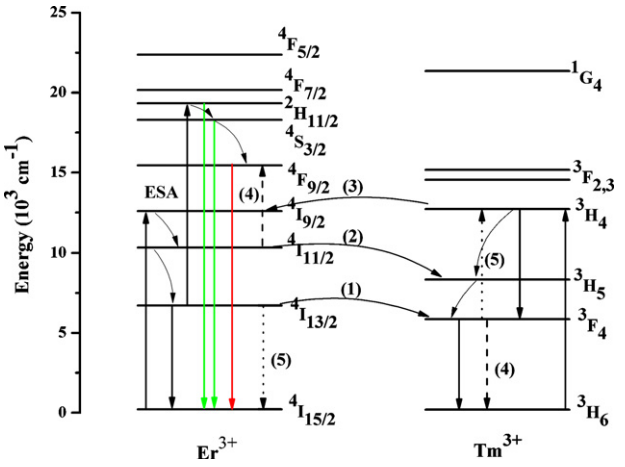

Fig. 6. Schematic energy level diagram and emission mechanism of Er^{3+} and Tm^{3+} ions, together with the involved ET processes between them.

ture. The excitation wavelength was 800 nm and the $^3H_6$ level and $^4I_{15/2}$ level were excited directly. It is obviously from Fig. 5 that both the emission intensity of 1.46 μm and 1.53 μm depend on the temperature, nevertheless, in lower temperature below 100 K, it is almost no change for the emission intensities for both the $^3H_4 \rightarrow {}^3F_4$ (1.46 μm) and $^4I_{13/2} \rightarrow {}^4I_{15/2}$ (1.53 μm) transitions. In higher temperature above 100 K, the emission intensities decrease with the increasing of temperature, and it can be noted that the emission intensity of 1.53 μm deceases much drastical than that of 1.46 μm, and the two intensities become nearly equal to unity at 300 K. The temperature dependence of the emission spectra can be understood by considering the phonon assistant energy transfer (ET) rate, which is given by Miyakawa–Dexter theory [28,29],

$$W_{ETR}(\Delta E) = W_{ETR}(0)\exp(-\beta_T \Delta E) \quad (2)$$

where $W_{ETR}(0)$ represents phonon assisted ET rate at $\Delta E = 0$, ΔE is the energy difference between Tm^{3+} and Er^{3+} energy levels. β_T is the function of the phonon energy and electron–phonon coupling strength, which is proportional to temperature. Therefore, according to Eq. (2), the ET rate between Tm^{3+} and Er^{3+} ions increases with temperature from 10 K to 300 K, which also agree well with the measured lifetimes of $^4I_{13/2}$ and $^3H_4$.

The temperature dependence of the broadband emission spectra can be helpful to understand the energy transfer processes between Tm^{3+} and Er^{3+} in BGN glasses, which is shown in Fig. 6. First, 800 nm excitation of Tm^{3+} and Er^{3+} populates $^3H_4$ and $^4I_{9/2}$ levels from the ground states Tm^{3+}:$^3H_6$ and Er^{3+}:$^4I_{15/2}$, respectively. The relaxation in Tm^{3+} from $^3H_4 \rightarrow {}^3F_4$ level yields 1460 nm emission, whereas the Er^{3+} ions multiphonon relaxation to $^4I_{11/2}$ level then to $^4I_{13/2}$ generating 1530 nm emission. On the other hand, excited state absorption (ESA) from $^4I_{13/2}$ to $^2H_{11/2}$ can occur. The dominant energy transfers are described as below [3,8,29]:

$$ET1: Er^{3+}{:}{}^4I_{13/2}, Tm^{3+}{:}{}^3H_6 \rightarrow Er^{3+}{:}{}^4I_{15/2}, Tm^{3+}{:}{}^3F_4$$

$$ET2: Er^{3+}{:}{}^4I_{11/2}, Tm^{3+}{:}{}^3H_6 \rightarrow Er^{3+}{:}{}^4I_{15/2}, Tm^{3+}{:}{}^3H_5$$

$$ET3: Tm^{3+}{:}{}^3H_4, Er^{3+}{:}{}^4I_{15/2} \rightarrow Tm^{3+}{:}{}^3H_6, Er^{3+}{:}{}^4I_{9/2}$$

$$ET4: Tm^{3+}{:}{}^3F_4, Er^{3+}{:}{}^4I_{11/2} \rightarrow Tm^{3+}{:}{}^3H_6, Er^{3+}{:}{}^4F_{9/2}$$

$$ET5: Er^{3+}{:}{}^4I_{13/2}, Tm^{3+}{:}{}^3F_4 \rightarrow Er^{3+}{:}{}^4I_{15/2}, Tm^{3+}{:}{}^3H_4$$

In low temperature, the ET1 process could happen most likely because it will release phonons [29]. In higher temperature above 100 K, as more phonons are available, the ET5 process would be more possible to happen while the ET1 process would be correspondingly suppressed. Therefore, the fluorescence lifetime of Er^{3+}:$^4I_{13/2}$ increases monotonically with the increasing of measuring temperature. The ET3 process, which is a resonant energy transfer because of a very small gap between the Er^{3+}:$^4I_{13/2}$ and Tm:$^3H_4$ levels, depopulates Tm^{3+}:$^3H_4$ level, resulting in the reduction of the emission intensity and lifetime at 1460 nm. These results would be helpful to fully understand the energy transfer between Er^{3+} and Tm^{3+} and achieve a flat and broadband emission at different temperature in bismuthate glasses.

4. Conclusions

In summary, Er^{3+}–Tm^{3+} co-doped novel bismuthate glasses with different [Tm]/[Er] ratios have been synthesized by conventional melt-quenching method. A fairly flat and broad emission covering the wavelength range of 1300–1650 nm corresponding to the $^3H_4 \rightarrow {}^3F_4$ transition of Tm^{3+} and $^4I_{13/2} \rightarrow {}^4I_{15/2}$ transition of Er^{3+} can be observed with the excitation of 800 nm laser. A full width at half maximum (FWHM) of ~160 nm is obtained by codoping the glass with 1.0 wt% of Tm_2O_3 and 0.3 wt% of Er_2O_3. The energy transfer processes between Tm^{3+} and Er^{3+} in BGN glasses are analyzed in detail. The temperature dependence of the broadband emission spectra in Er^{3+}–Tm^{3+} co-doped BGN glass is also studied, which is helpful to understand the energy transfer processes. The present work indicates that Er^{3+}–Tm^{3+} co-doped BGN glasses can be promising materials for broadband light sources and broadband amplifiers for WDM transmission systems.

Acknowledgements

This research was financially supported by the Chinese National Natural Science Foundation (grant 60607014 and grant 50672107) and the Chinese National 863 Project (No. 2007AA03Z441).

References

[1] H. Jeong, K. Oh, S.R. Han, T.F. Morse, Chem. Phys. Lett. 367 (2003) 507.
[2] L.D. Labio, W. Lüthy, V. Romano, F. Sandoz, T. Feurer, Appl. Opt. 47 (2009) 1581.
[3] R. Balda, J. Fernández, J.M. Fernández-Navarro, Opt. Exp. 17 (2009) 8781.
[4] H. Jeong, K. Oh, S.R. Han, T.F. Morse February, Opt. Lett. 28 (2003) 161.
[5] S.Y. Seo, J.H. Shin, B.S. Bae, N. Park, J.J. Penninkhof, A. Polman, Appl. Phys. Lett. 82 (2003) 3445.
[6] M. Semenkoff, M. Guibert, V. Ronarch, Y. Sorel, J.F. Kerdiles, J. Non-Cryst. Solids 184 (1995) 240.
[7] Y. Xu, D. Chen, W. Wang, Q. Zhang, H. Zeng, C. Shen, G. Chen, Opt. Lett. 33 (2008) 2293.
[8] L. Huang, A. Jha, S. Shen, X. Liu, Opt. Exp. 12 (2004) 2429.
[9] D. Zhou, Z. Song, G. Chi, J. Qiu, J. Alloys Compd. 481 (2009) 881.
[10] D. Chen, Y. Wang, F. Bao, Y. Yu, J. Appl. Phys. 101 (2007) 113511.
[11] A. Pan, A. Ghosh, Phys. Rev. B 62 (2000) 3190.
[12] H. Fan, G. Gao, G. Wang, J. Hu, L. Hu, Opt. Mater. 32 (2010) 627.
[13] A. Pan, A. Ghosh, J. Non-Cryst. Solids 271 (2000) 157.
[14] Y.B. Saddeek, K.A. Aly, A. Dahshan, I.M.El. Kashef, J. Alloys Compd. 494 (2010) 210.
[15] A.A. Bahgat, B.A.A. Makram, E.E. Shaisha, M.M. El-Desoky, J. Alloys Compd. 506 (2010) 141.
[16] Y. Xu, Q. Zhang, C. Shen, D. Chen, H. Zeng, G. Chen, J. Am. Ceram. Soc. 92 (2009) 3088.
[17] S. Ohara, Y. Kuroiwa, Opt. Exp. 17 (2009) 14104.
[18] S. Hazra, A. Ghosh, Phys. Rev. B 51 (1995) 851.
[19] S. Hazra, S. Mandal, A. Ghosh, Phys. Rev. B 56 (1997) 8021.
[20] A. Pan, A. Ghosh, J. Mater. Res. 17 (2002) 1941.
[21] B.R. Judd, Phys. Rev. 127 (1962) 750.
[22] G.S. Ofelt, J. Chem. Phys. 37 (1962) 511.
[23] C.K. Jorgensen, R. Reisfeld, J. Less-Common Met. 93 (1983) 107.
[24] Y. Yang, Z. Yang, B. Chen, P. Li, X. Li, Q. Guo, J. Alloys Compd. 479 (2009) 883.
[25] S. Ivanova, F. Pellé, J. Opt. Soc. Am. B 26 (2009) 1930.
[26] N. Jaba, H.B. Mansour, B. Champagnon, Opt. Mater. 31 (2009) 1242.
[27] K. Li, Q. Zhang, G. Bai, S. Fan, J. Zhang, L. Hu, J. Alloys Compd. 504 (2010) 573.
[28] T. Miyakawa, D.L. Dexter, Phys. Rev. B 1 (1970) 2961.
[29] H. Lou, X. Wang, Z. Tao, F. Lu, Z. Jiang, L. Mai, F. Xu, Appl. Surf. Sci. 255 (2009) 8217.